From frequency dispersion to ohmic impedance: A new insight on the high-frequency impedance analysis of electrochemical systems

Oumaïma Gharbi, Arthur Dizon, Mark Orazem, Tran Mai, Bernard Tribollet, Vincent Vivier

From Frequency Dispersion to Ohmic Impedance: A New Insight on The High-Frequency Impedance Analysis of Electrochemical Systems

Oumaïma Gharbi,[1] Arthur Dizon,[2] Mark Orazem,[2] Mai T.T. Tran,[1] Bernard Tribollet,[1] and Vincent Vivier[1,*]

[(1)] Sorbonne Université, CNRS, Laboratoire Interfaces et Systèmes Electrochimiques, LISE, F-75005 Paris, France

[(2)] Department of Chemical Engineering, University of Florida, Gainesville, FL, 32611 USA

Abstract

The increasing use of impedance for the characterization of an electrified interface is accompanied by the development of accurate models to analyze the results. In the present work, the concept of ohmic impedance is revisited using both numerical simulations and experimental results. The Havriliak-Negami equation is shown to provide a good representation of the high-frequency dispersion or complex ohmic impedance associated with the disk electrode geometry. An excellent fit to simulated complex ohmic impedance was found for both capacitive electrodes and for electrodes characterized by constant-phase-element behavior. The use of the Havriliak-Negami equation to account for the complex ohmic impedance was shown to extend the useful frequency range for regression of physical models to the impedance response for three experimental systems: a gold electrode in a 0.1 M sodium sulfate solution, an aluminum electrode in a 0.01 M sodium sulfate solution, and pure iron in a 0.5 M sulfuric acid solution.

Keywords: Electrochemical impedance spectroscopy (EIS); Constant-phase-element (CPE); Complex nonlinear regression; Physical models; Distributed circuit element

Corresponding author: vincent.vivier@sorbonne-universite.fr

1. Introduction

In his seminal work on the simulation of the impedance response of a blocking electrode (i.e., with a pure capacitance as governing interfacial boundary condition), Newman introduced the concept of frequency dispersion[1-2] accounting for the effect of electrode geometry on the primary current distribution. This frequency dispersion was explained by the variations in capacitance at high frequencies, caused by the non-uniform primary current distribution at the periphery of the electrode (i.e., the boundary between the insulator and the conductive part of the electrode). Conversely, in low frequencies, the current distribution becomes uniform, leading to a constant value of the capacitance with frequency.

Newman's approach has been revisited for different cases, including an ideally blocking electrode,[3] a blocking electrode with a local constant-phase element behavior,[4] and a disk electrode with faradaic reactions.[5-6] It was shown using both numerical simulations and local electrochemical impedance spectroscopy (LEIS) experiments performed on a stainless steel passive electrode, that the frequency dispersion results in an ohmic impedance with a non-zero imaginary component at the high frequencies.[7] The term ohmic impedance was introduced in 2007 to describe a transfer function associated with the resistance of the electrolyte to passage of current under the influence of geometry-induced (and frequency-dependent) non-uniform current and potential distributions.[3] Interestingly, the concept of an ohmic impedance, which accounts for the same phenomenon of frequency dispersion described by Newman, made it possible to extend the concept of local impedance in terms of the sum of the local interfacial impedance, measured locally just outside the double layer, and the local ohmic impedance.[8-10]

Moreover, the development of LEIS has allowed the experimental validation of the ohmic impedance concept.[10-12] In fact, the influence of electrochemical cell geometry has been observed experimentally through the use of recessed electrodes in which the LEIS response as a function of the probe position along the electrode radius has been measured.[13] These experiments showed that the frequency dispersion caused by the electrode geometry can be cancelled by using a recessed electrode at least twice deeper than the electrode diameter. Such an electrode geometry can be easily used, for instance when working on the electrochemical characterization of coatings.[14] However, when careful control of the hydrodynamics in the system is required to evacuate the products from the electrode/electrolyte interface (e.g., with a rotating-disk electrode), or to work

with a small electrode size, such a configuration is no longer possible. Additionally, all these features (inductive and capacitive time constants) observed at the high frequencies of the local impedance response always result in a capacitive time constant on the global impedance response corresponding to the so-called frequency dispersion.

From a practical point of view, most of the experiments reported in the literature deal with global impedance measurements and neglect the contributions of current and potential distributions. This is certainly due to the fact that consideration of these contributions requires simultaneous solution of the interfacial kinetics and Laplace's equation in the electrochemical cell, which complicates analysis of the results as compared to what can be done with equivalent electrical circuits. However, the analysis of the high-frequency domain is required for any electrochemical system considered and is of special interest for many practical applications dealing with the detailed analysis of capacitive behavior of an electrode such as supercapacitors,[15] semiconductors (e.g. Mott-Schottky analysis),[16] thin oxide films,[17-18] or coatings for material protection.[19-20] Interpretation of impedance measurements thus requires a good understanding of the processes in the high-frequency domain, including its ohmic component.

In the present work, particular attention is paid to the ohmic contribution observed in the high-frequency domain both for capacitive and faradaic electrochemical responses. A detailed description of the ohmic impedance is introduced, first based on synthetic data in order to devise an analytical expression as a quantity that can be used easily in any fitting procedure. In a second step, the experimental validation of this new development is presented, to exemplify the utility of the detailed analysis of the high frequencies for a correct description of the capacitive contribution of the electrochemical impedance.

2. Experimental

Three different electrochemical systems were investigated in this work in order to provide a detailed description of the ohmic impedance in the high frequencies. The response of a blocking electrode with a local constant phase element (CPE) was investigated using a gold disk-electrode of 5 mm in diameter in a 0.1 M deaerated sodium sulfate solution (Na_2SO_4). The electrode was first cycled over the oxidation and reduction limits of the solvent and then biased at E = -0.250 V/MSE (MSE: mercury sulfate electrode – E_{MSE} = 0.64 V/SHE) for performing the EIS measurement. The CPE response due to a thin oxide film was studied using pure aluminum as an

electrode material. The experiments were performed using a 8 mm diameter disk electrode in 0.01 M Na_2SO_4 solution after two-hour immersion at the corrosion potential (E = -1.19 V/MSE), thus allowing formation of a few nanometer thick aluminum oxide film. The electrochemical response of a faradaic system was investigated using the dissolution of pure iron in a 0.5 M sulfuric acid solution. A 5 mm diameter iron disk-electrode biased at E = -0.924 V/MSE was used for performing the EIS measurement under air atmosphere.

The experiments on gold and aluminum electrodes were performed with a Gamry Reference 600+ potentiostat. The iron dissolution was studied with a Sotelem potentiostat coupled to a frequency response analyzer (Solartron 1255). All the experiments were performed at room temperature (20 ±1°C).

All the simulations were performed using finite-element methods (FEM). The 2-D axisymmetric solution to Laplace's equation in cylindrical coordinates was obtained numerically using COMSOL Multiphysics® 5.0. The hardware used for simulation was a 64-bit Dell™ Precision T7500 workstation with dual Intel® Xeon® E5620 2.4 GHz processors and 96 GB of RAM.

3. Model

In order to account for current and potential distributions on the impedance response of an electrochemical system, the potential distribution must be calculated for the entire electrochemical cell. For simplicity, the mathematical development is devised for a planar disk electrode embedded in a coplanar insulator, which corresponds, in fact, to one of the most widely used electrochemical setups. Therefore, the geometry of the system is defined by the electrode radius, r_0, and the distribution of potential Φ in solution is governed by Laplace's equation, which is expressed in cylindrical coordinates as

$$\frac{1}{r}\frac{\partial}{\partial r}\left(r\frac{\partial \Phi}{\partial r}\right)+\frac{\partial^2 \Phi}{\partial y^2}=0 \qquad \textit{Eq. 1}$$

where r is the radial coordinate and y is the normal distance to the electrode surface.

In this section, the model will be devised for small amplitude sinewave perturbation signal in the case of a blocking electrode either with a pure capacitance or with a local constant-phase element behavior. Thus, at the electrode surface, the flux boundary condition is

$$-\kappa\frac{\partial \Phi}{\partial y}\Big|_{y=0}=Q(j\omega)^{\alpha}(V-\Phi_0) \qquad \textit{Eq. 2}$$

where κ is the electrolyte conductivity, α and Q are the CPE parameters ($\alpha = 1$ in the case of a pure capacitance), ω is the angular frequency of the sinewave perturbation, V is the electrode potential, and Φ_0 is the potential just outside the double layer.

On the surrounding insulator, the flux is equal to zero

$$\left.\frac{\partial \Phi}{\partial y}\right|_{y=0} = 0 \qquad for\ r > r_0 \qquad\qquad Eq.\ 3$$

and far from the electrode surface, the potential tends towards the reference electrode potential, which was set at zero for all the simulations.

$$\Phi \to 0 \quad as \quad (r^2 + y^2) \to \infty \qquad\qquad Eq.\ 4$$

These equations were solved using the finite-element method, as previously described.[10, 21]

As the complex ohmic impedance obtained from numerical simulation requires subtraction of the interfacial impedance from the calculated impedance, a refined numerical solution is required. The simulation domain was chosen to be an axisymmetric hemisphere, where the center of the embedded disk electrode was located at the coordinates $r = 0$ and $y = 0$. The meshing parameters of the simulation were the radius of the hemisphere H_{dom}, the maximum element size on the surface of the electrode s_{surf}, and the element size at the edge of the disk s_{edge}. The domain and meshing parameters were determined iteratively such that the resistance obtained from the calculation of the primary current distribution was in agreement with the analytic solution for ohmic resistance of a disk electrode developed by Newman expressed in dimensionless form as $R_{\mathrm{e}}\kappa/\pi r_0 = 0.25$.[22] The final domain and meshing parameters were $H_{\mathrm{dom}} = 3000 r_0$, $s_{\mathrm{edge}} = 4.5\times10^{-6} r_0$, and $s_{\mathrm{surf}} = 750 s_{\mathrm{edge}}$. The simulations required 5,547 domain elements and 487 boundary elements and had an average runtime of 47 s. The simulations yielded a dimensionless ohmic resistance of 0.2500023, which corresponded to a simulation error of 0.00092%.

4. Numerical Results

The impedance responses in the case of a pure capacitance and a local CPE are presented in Figure 1a in a Nyquist representation. Model parameters are given in Table 1. To facilitate comparison, EIS data were scaled by the ratio $\frac{\kappa}{r_0\pi}$, and frequency was made dimensionless using

$$K = \frac{Q\omega^{\alpha} r_0}{\kappa} \qquad Eq.\ 5$$

As expected, high-frequency dispersion was observed for all three cases,[3-4] and can be better seen using a semi-logarithmic representation of the EIS data as shown in Figure 1b in the case of the pure capacitance or with a zoom in the HF domain in the case of a CPE behavior as shown in Figure 1c. This frequency dispersion is visible for values of K greater than 1, that is for frequency *f* greater than 320 Hz, using $r_0 = 0.25$ cm, $\kappa = 0.005$ S·cm^{-1}, and $C = 10{\times}10^{-6}$ F·cm^{-2}, which are values commonly encountered experimentally. Such frequency dispersion can lead to misreading both the electrolyte resistance and the double layer capacitance. Indeed, Figure 1b shows that, depending on the frequency domain investigated, two values can be defined for the electrolyte resistance: R_{HF} in the high frequencies which formally corresponds to the primary electrolyte resistance defined by Newman,[22] and R_{LF} from the measurement of the real part of impedance in low frequencies. It should also be mentioned that in the case of a CPE behavior ($\alpha < 1$), the semi-logarithmic representation given in Figure 1b obscures frequency dispersion because, for a CPE, both the real and the imaginary component of the impedance varies with the frequency, but R_{HF} and R_{LF} can be obtained from the extrapolation of the two linear domain on the real axis, as shown in Figure 1c.

Table 1. Model parameters used to generate Figures 1 and 2.

α	1	0.85	0.7
r_0 [cm]	0.25	0.25	0.25
ρ [Ω cm]	200	200	200
Q [μF s$^{\alpha}$ cm^{-2}]	10	100	100

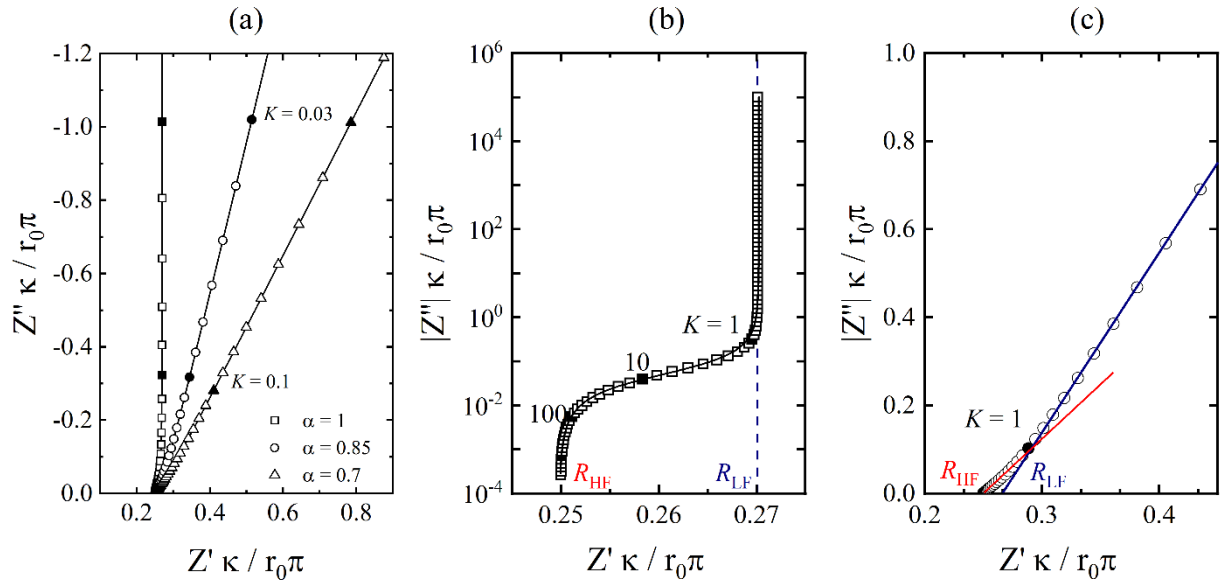

Figure 1: Simulated impedance response for model parameters given in Table 1: (a) Nyquist representation for the calculated impedance response of a blocking electrode with a pure capacitance (squares) and a local CPE (circles and triangles); (b) logarithmic scale showing the high-frequency distribution in the case of the pure capacitive electrode; (c) and zoom in the HF domain (linear scale) showing the high-frequency distribution in the case of the CPE behavior (α = 0.85). The impedances and the frequency are made dimensionless (see text), and the line represents the fit of equation (9) with fitting parameters given in Table 4.

From these synthetic data, the impedance attributed to frequency dispersion can be readily obtained as the difference between the impedance Z, calculated from the resolution of Laplace's equation and taking into account frequency dispersion, and the interfacial impedance calculated with the same value of the parameters but using an electrical equivalent circuit. This impedance corresponds to the definition of the ohmic impedance Z_e which can be expressed as

$$Z_e = Z - \frac{1}{Q(j\omega)^{\alpha}} \qquad \textit{Eq. 6}$$

Figure 2 shows the ohmic impedance response in a Nyquist representation for a pure capacitance (squares) and for a local CPE (circles and triangles) calculated from the set of synthetic data presented in Figure 1a. In both cases, this frequency dispersion results in a depressed capacitive contribution with a dimensionless high-frequency limit $R_{HF} = 0.25$ corresponding to the primary electrolyte resistance calculated by Newman[22] and a dimensionless low-frequency limit at about $R_{LF} = 0.27$, thus resulting in a variation of 8% of the real part of the impedance over the entire frequency domain. Additionally, the degree of flattening of the loop clearly depends on the interfacial boundary conditions (i.e., the value of α), but the main result is that the ohmic

contribution to the global electrochemical impedance response is indeed described by a complex impedance.

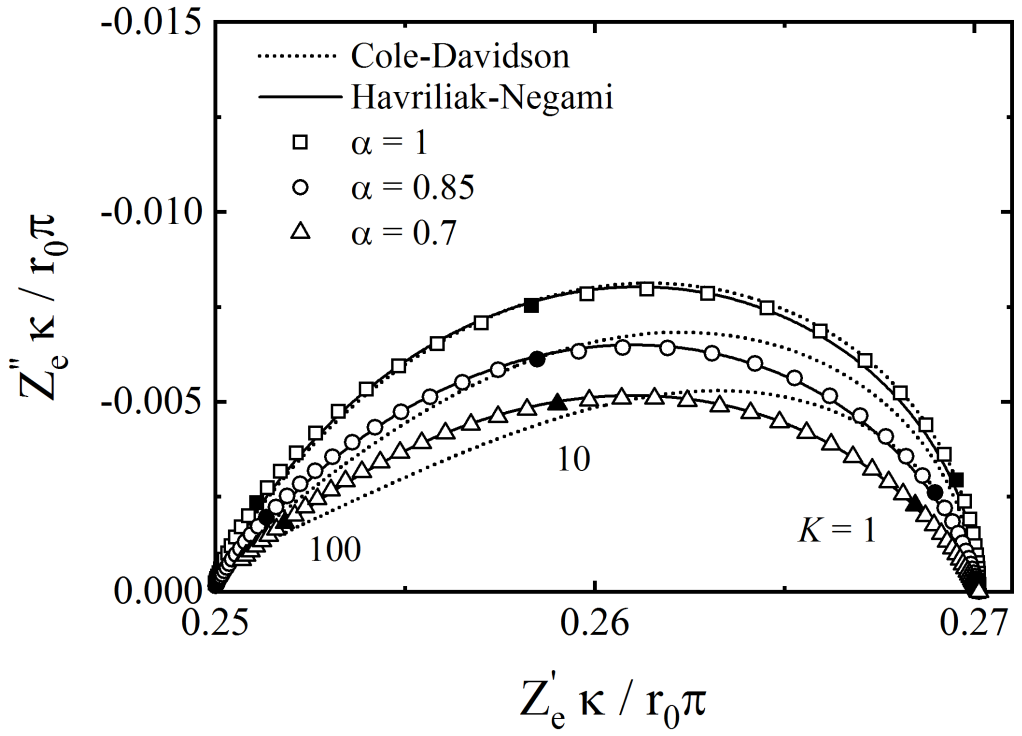

Figure 2: Nyquist representation ohmic impedance, Z_e, determined for the calculated impedance response of a blocking electrode with a pure capacitance (squares) and a local CPE (circles and triangles) presented in Figure 1. The dotted lines correspond to the fitting of each impedance diagram with the Cole-Davidson equation (7), and the solid lines correspond to the fitting by the Havriliak-Negami equation (8). Fitting results are presented in Table 2.

Interestingly, a large amount of work on dielectric relaxation has been done for describing the non-ideal behavior observed in solid-state impedance specroscopy.[23-25] The shape of the ohmic impedance presented in Figure 2 is consistent with either a Cole-Davidson expression

$$Z_e = R_{HF} + \frac{R_{LF}-R_{HF}}{(1+j\omega\tau)^{\beta}} \qquad Eq.\ 7$$

where R_{HF} and R_{LF} are the high- and low-frequency limits of the resistive behavior, respectively, and τ and β are the two parameters corresponding to the distribution of time constant; or with the Havriliak-Negami equation,[26]which may be expressed as

$$Z_e = R_{HF} + \frac{R_{LF}-R_{HF}}{(1+(j\omega\tau)^{\upsilon})^{\beta}} \qquad Eq.\ 8$$

in which a third parameter υ is introduced to account for frequency dispersion.

As shown in Figure 2, both the Cole-Davidson and Havriliak-Negami equations allow a good fit of the results for the capacitive electrode, and in both cases, the value of R_{HF} and R_{LF} correspond to the resistive contributions introduced in Figure 1b. However, the Havriliak-Negami equation provides a better fit to the synthetic data associated with a CPE and even provides a slightly better fit for the capacitive electrode (Table 2). The value of the term υ introduced in the Havriliak-Negami equation and determined from the fitting procedure is loosely associated with the α coefficient of the CPE ($\alpha = 1$ for an ideal capacitance). Such a result makes sense since the CPE behavior should be observed independently of the frequency dispersion due to the geometry of the electrode; whereas, the term β used in both relationships accounts for the frequency dispersion itself.

Table 2. Results of Levenberg-Marquardt regression of equations (7) and (8) to the synthetic ohmic-impedance data presented in Figure 2 under modulus weighting. Confidence intervals represent ±1σ.

		$\alpha = 1$	$\alpha = 0.85$	$\alpha = 0.7$
Cole-Davidson Equation (7)	$R_{HF}\kappa/r_0\pi$	0.249610 ± 0.000026	0.249230 ± 0.000085	0.24677 ± 0.00035
	$R_{LF}\kappa/r_0\pi$	0.270110 ± 0.000011	0.269980 ± 0.000033	0.269910 ± 0.000043
	τ [μs]	117.40 ± 0.88	542 ± 13	212.0 ± 9.5
	β	0.380 ± 0.003	0.550 ± 0.007	0.750 ± 0.009
Haviliak-Negami Equation (8)	$R_{HF}\kappa/r_0\pi$	0.24970 ± 0.00002	0.24973 ± 0.00002	0.24952 ± 0.00002
	$R_{LF}\kappa/r_0\pi$	0.27014 ± 0.00001	0.27014 ± 0.00001	0.27013 ± 0.00001
	τ [μs]	106.0 ± 1.1	310.0 ± 3.7	60.5 ± 0.6
	υ	0.962 ± 0.003	0.817 ± 0.002	0.683 ± 0.002
	β	0.683 ± 0.006	0.690 ± 0.005	0.649 ± 0.004

To reduce the number of parameters used in the model, the term υ in Equation 8 was replaced by the value of α, e.g., $\alpha = 1$, $\alpha = 0.85$, and $\alpha = 0.7$ for the synthetic data presented in Figure 2. The fit was indistinguishable from that shown in Figure 2, and the regression parameters are shown in Table 3. The modification of Equation 8 provides an adequate representation of the complex ohmic impedance. The adjusted value of β was between 0.6 and 0.63.

Table 3. Results of Levenberg-Marquardt regression of equation (8) assuming ν equal to α, to the synthetic data presented in Figure 2 under modulus weighting. Confidence intervals represent $\pm 1\sigma$.

	$\alpha = 1$	$\alpha = 0.85$	$\alpha = 0.7$
$R_{HF}\kappa/r_0\pi$	0.24961 ± 0.00003	0.24964 ± 0.00002	0.24938 ± 0.00002
$R_{LF}\kappa/r_0\pi$	0.27011 ± 0.00001	0.27011 ± 0.00001	0.27011 ± 0.00001
τ [μs]	117.35 ± 0.88	352.8 ± 2.9	68.12 ± 0.47
ν	1 (fixed)	0.85 (fixed)	0.7 (fixed)
β	0.6251 ± 0.0034	0.6309 ± 0.0032	0.6049 ± 0.0025

Thus, for a blocking electrode, the overall impedance Z is obtained as the sum of the ohmic impedance and the interfacial capacitance which can be expressed in the most general way by a CPE as

$$Z = Z_e + Z_{CPE} = R_{HF} + \frac{R_{LF} - R_{HF}}{(1+(j\omega\tau)^{\alpha})^{\beta}} + \frac{1}{Q(j\omega)^{\alpha}} \qquad Eq.\ 9$$

Equation (9) was used for the fitting of the synthetic data presented in Figure 1. The results are presented as lines in Figure 1, and the fitted parameters are reported in Table 4. It can be seen that the use of equation (9) allows a fit of the impedance data over the whole frequency range for both for the pure capacitance and the CPE. Moreover, from the results of the confidence intervals reported in Table 2, all the parameters can be determined with a good accuracy, even for the capacitive system, thus validating the choice of the Havriliak-Negami equation and the number of parameters used to analyze the results. It should be mentioned that the errors reported in Table 2 are estimates since the Cole-Davidson and Havriliak-Negami models are approximate models that yield reasonable fits. For a pure-capacitive behavior both models are indistinguishable; whereas, a CPE behavior prompts the use of the Havriliak-Negami model because of lower regression error.

A result of this numerical analysis is that the β parameter introduced in equation (9) is on the order of $0.65 - 0.70$ for both capacitive and CPE blocking electrodes, and thus corresponds to the frequency dispersion due to the geometry of the electrode. It should however be mentioned that this analysis requires data that can be used in high frequencies, and that the frequency domain on which the frequency dispersion is observed is for $K > 1$, that is for values depending on the electrode size and the electrolyte conductivity (see equation (5)).

Table 4. Results of Levenberg-Marquardt regression of equation (9) to the synthetic data presented in Figure 1 under statistical weighting. Confidence intervals represent ±1σ.

	α = 1			α = 0.85			α = 0.7		
$R_{HF}\kappa/r_0\pi$	0.24994	±	0.00007	0.249898	±	0.000051	0.24967	±	0.00003
$R_{LF}\kappa/r_0\pi$	0.26995	±	0.00007	0.269746	±	0.000083	0.269890	±	0.000042
τ / μs	98.2	±	1.6	278.9	±	5.0	57.5	±	0.8
α	1.000000	±	0.0000002	0.850000	±	0.000003	0.69999	±	0.00001
β	0.6965	±	0.0044	0.7012	±	0.0037	0.6506	±	0.0028
Q /μFs^{α}cm^{-2}	9.9949	±	0.0001	99.9995	±	0.00094	100.013	±	0.0010

It can also be of interest to perform the analysis of the impedance data using other representations such as the complex capacitance plot,[17] as shown on Figure 3 for the synthetic data presented in Figure 1, using the mathematical transformation of the impedance

$$C^* = \frac{1}{j\omega(Z - Z_e)} \qquad \textit{Eq. 10}$$

where C^* is the complex capacitance which is expressed as $C^* = C' + jC''$. Correction by the high-frequency ohmic resistance yields a loop that approaches the correct value of the real part of the capacitance only at low frequency. Correction by the ohmic impedance, however, yields a real part of the capacitance that is the correct value for all frequencies. The complex capacitance representation allows the high-frequency capacitance to be obtained, but as shown on Figure 3, the error for estimation of capacitance can be a factor of 2 if the ohmic contribution is not properly corrected.

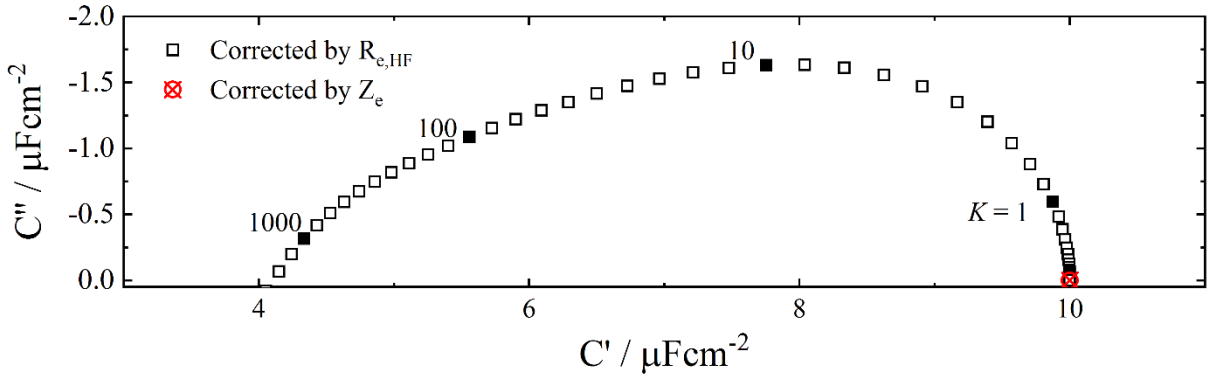

Figure 3: Determination of the interfacial capacitance from the capacitance plot calculated for the blocking electrode shown in Figure 1 with a pure capacitance (C = 10 µF cm^{-2}) corrected by the high-frequency value of the impedance (squares) and corrected by the ohmic impedance, Z_e (⊗).

5. Experimental Results and Discussion

Three different examples demonstrate that the correction of the ohmic contribution, when done correctly, facilitates extraction of information from the high-frequency part of impedance diagrams. The systems considered include a gold electrode in a 0.1 M sodium sulfate solution, an aluminum electrode in a 0.01 M sodium sulfate solution, and pure iron in a 0.5 M sulfuric acid solution.

5.1 Gold Electrode

Figure 4 shows the electrochemical impedance response of a 5 mm diameter gold disk-electrode immersed in a 0.1 M deaerated sodium sulfate solution and biased in the double layer region at *E* = -0.250 V/MSE in the frequency domain ranging from 100 kHz and 0.1 Hz. The impedance diagram shows a capacitive behavior (Figure 4a) for which the frequency dispersion is masked in the high-frequency domain if only raw data are plotted (Figure 4c). Following the seminal work of Orazem et al. for calculating the corrected phase angle using the electrolyte resistance,[27] the corrected phase angle was obtained from the global impedance corrected from the ohmic impedance as

$$\varphi_{corr} = tan^{-1}\left(\frac{(Z-Z_e)''}{(Z-Z_e)'}\right) \qquad Eq.\ 11$$

Where $(Z-Z_e)'$ and $(Z-Z_e)''$ are the real and the imaginary part of the global impedance corrected by the ohmic impedance, respectively. It is worth noting that the representation of the corrected phase as a function of the frequency (Figure 4d) is the only way to clearly see the CPE

behavior in a large frequency domain, including at high frequency. Such a behavior corresponds to a blocking electrode with a CPE behavior as already observed in the literature[28] and can be analyzed using equation (9). The fitting of the results allows the ohmic impedance to be calculated (Figure 4b). Additionally, the phase angle variation as a function of the frequency shows a constant value in the whole high-frequency domain when the data are corrected by the ohmic impedance (Figure 4d). In this case, the corrected phase angle corresponds to 82°, equivalent to a value of $\alpha = 0.91$ for the CPE; whereas, the β parameter determined from the fitting procedure is 0.62, which is in good agreement with the theoretical derivation for blocking electrodes presented in the former section. Thus, the frequency dispersion is described by the parameter β and is attributed to the geometry of the electrode. Therefore, the CPE behavior observed when data are corrected by the ohmic impedance correspond to the double layer capacitance which can be analyzed using Brug's formula[29-30] to convert the CPE to a real capacitance (c.a. 11.3 μFcm^{-2}), thus taking into account the surface distribution of the impedance.

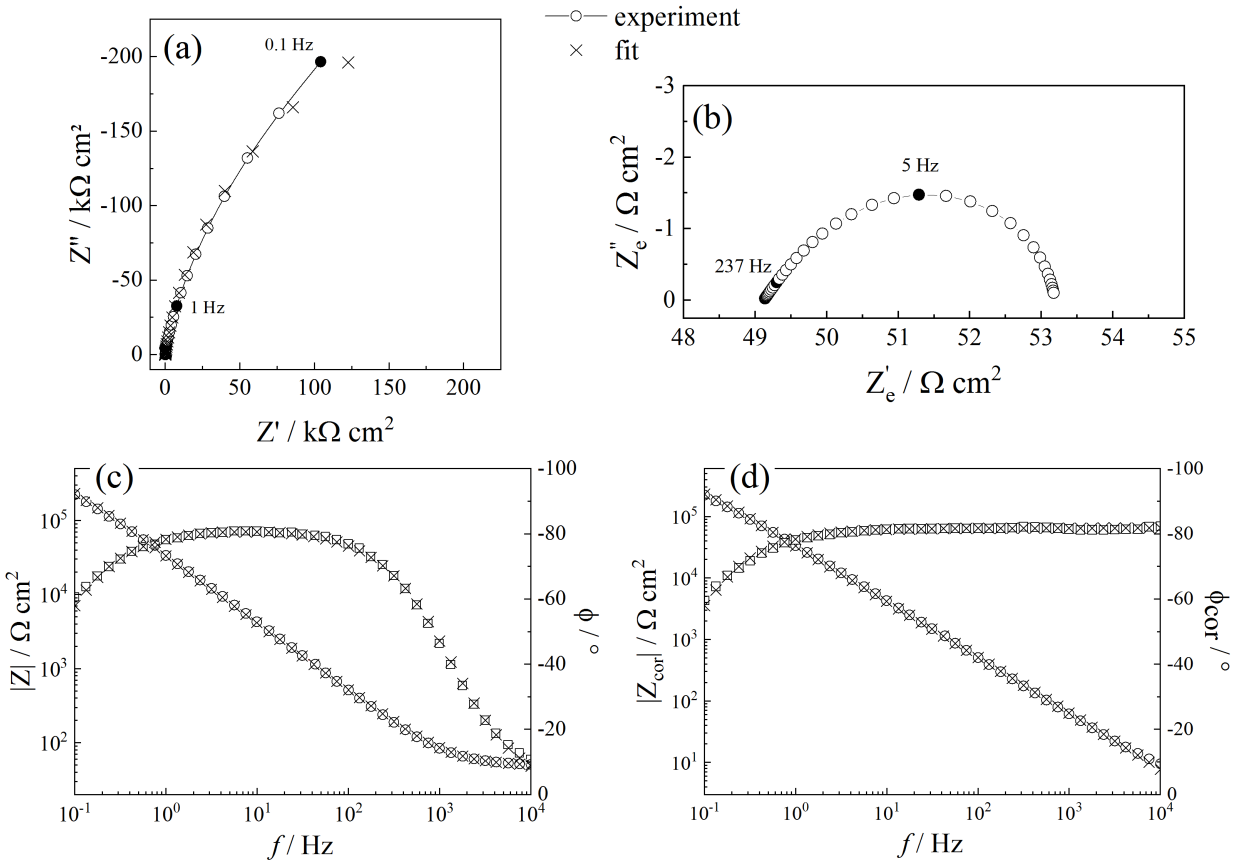

Figure 4: Electrochemical impedance response of a gold disk-electrode of 5 mm in diameter in a 0.1 M sodium sulfate solution biased at E = -0.250 V/MSE. (a) Nyquist representation of the impedance; (b) Nyquist representation of the ohmic impedance; (c) Bode representation of the impedance – raw data (d) Bode representation of the impedance – corrected by the ohmic impedance.

The open symbols correspond to the experimental data and the crosses correspond to the fitting of the EIS response with the model proposed in this work (equation (9)).

5.2 Aluminum Electrode

High-frequency impedance analysis can also be performed on systems whose response follows a complicated relaxation law, such as the power-law model developed for describing the CPE behavior of a thin film.[19, 31-32] Figure 5 shows the impedance response of an aluminum electrode after 2h immersion at the corrosion potential and subsequent polarization at E = -1.19 V/MSE. The shape of the impedance diagram corresponds to a capacitive behavior attributed to the response of the thin oxide film formed at the aluminum surface, the dielectric properties of which being described by the power-law model as

$$Z_{oxide}(\omega) = \int_0^{\delta_{ox}} \frac{\rho(x)}{1+j\omega\varepsilon\varepsilon_0\rho(x)}\,dx \qquad \textit{Eq. 12}$$

in which ε is the oxide relative permittivity, ε_0 is the permittivity of vacuum, $\rho(x)$ is the local resistivity depending on normal coordinate, x, and δ_{ox} is the thickness of the film. The resistivity $\rho(x)$ can be expressed as a function of x as

$$\rho(x) = \rho_\delta \left[\frac{\rho_\delta}{\rho_0} + \left(1 - \frac{\rho_\delta}{\rho_0}\right)\left(\frac{x}{\delta_{ox}}\right)^\gamma\right]^{-1} \qquad \textit{Eq. 13}$$

where γ is the power-law parameter and ρ_0 and ρ_δ are the boundary values of the resistivity at the metal / oxide interface and at the oxide / solution interface, respectively.

Thus, the overall expression of the impedance used for the fit of the experimental results presented in Figure is

$$Z(\omega) = Z_e + Z_{oxide} = R_{HF} + \frac{R_{LF}-R_{HF}}{(1+(j\omega\tau)^\alpha)^\beta} + \int_0^{\delta_{ox}} \frac{\rho(x)}{1+j\omega\varepsilon\varepsilon_0\rho(x)}\,dx \quad \textit{Eq. 14}$$

It was previously shown that the value of γ is directly linked to the α parameter of the CPE describing the non-ideal behavior of the thin-film through

$$\alpha = \frac{\gamma-1}{\gamma} \qquad \textit{Eq. 15}$$

This relationship was used in equation (14) as the expression of the α parameter of the Havriliak-Negami contribution.

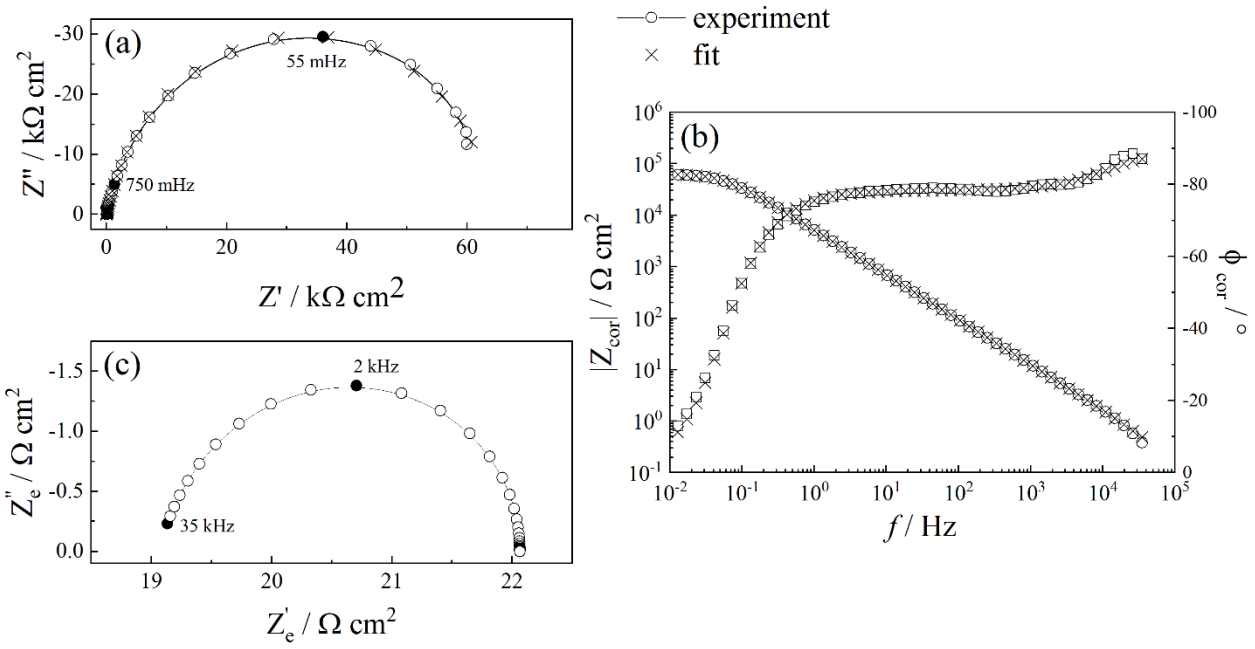

Figure 5: Electrochemical impedance response of an aluminum disk-electrode of 8 mm in diameter after two-hour immersion in a 0.01 M sodium sulfate solution and biased at E = -1.19 V/MSE. (a) Nyquist representation of the impedance; (b) Bode representation of the impedance corrected by the ohmic impedance; (c) Nyquist representation of the ohmic impedance. The red symbols correspond to the experimental data and the crosses correspond to the fitting of the EIS response with the model proposed in this work (equation (14)).

The results of the impedance fit are reported in Figure 5 and show a good agreement with the experimental data. Interestingly, the whole impedance spectrum is perfectly fitted with equation (14). Moreover, the ohmic contribution of the impedance can also be determined (Figure 5c). The variations in the corrected phase angle clearly show the interest of the method developed in this article. Indeed, when the raw phase is plotted as a function of the frequency, the presence of a hump in the high-frequency range masks the essential information of high-frequency capacitive behavior, similar to results shown in the case of a gold blocking electrode (Figure 4). When the phase is recalculated taking into account the ohmic impedance, CPE behavior is then clearly seen in the high-frequency domain with a phase that tends towards -90° in very high frequency. It should be noted that it is this last contribution that is analyzed when using the complex capacitance representation to determine the thickness of the oxide films formed on the surface of the electrodes.[17-18, 33] The β parameter determined from the fitting procedure is 0.77, and will be further discussed in the following section.

As expected with the refined correction of the ohmic impedance shown in equation (10), the complex capacitance plot calculated from the impedance response of the Al electrode in sodium sulfate solution shows a well-defined high-frequency domain (Figure 6a). From the extrapolation of the real part of the capacitance towards the infinite frequency, a high-frequency capacitance of 1.14 μFcm^{-2} is determined (Figure 6b). Assuming a dielectric permittivity of 11.5 for the thin oxide alumina film formed at the electrode surface, a film thickness of 9 nm is readily determined, which is in agreement with value usually encountered in the literature.[18]

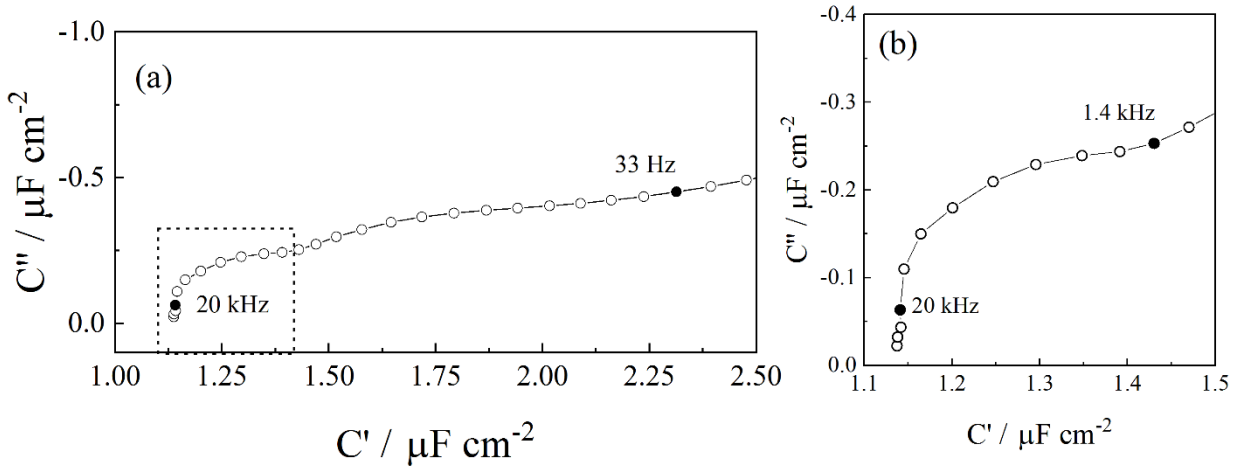

Figure 6: Determination of the interfacial capacitance from the capacitance plot calculated with equation (10) for impedance response of an aluminum disk-electrode shown in Figure 5. (a) Complex capacitance in a Nyquist representation; (b) Zoom on the high frequency domain of the complex capacitance plot.

5.3 Iron Electrode

The present impedance analysis can be extended to electrochemical systems with complex kinetics involving faradaic reactions. This is demonstrated in the case of the active dissolution of pure iron in sulfuric acid solution (0.5 M – pH = 0.3), for which a representative impedance diagram is presented in Figure 7. The impedance diagram shows a high-frequency capacitive loop, corresponding to the charge-transfer reaction in parallel to the interfacial capacitance, and a low-frequency inductive loop attributed to the relaxation of the adsorbed species. The anodic dissolution of pure iron is well-documented in the literature[34-35] and is in agreement with the impedance results reported in Figure 7. From a mechanistic point of view, the dissolution of iron can be described as a two-step electrochemical reaction involving an adsorbed intermediate, i.e.,

$$\mathrm{Fe} \xrightarrow{k_1} \mathrm{Fe}_{\mathrm{ads}}^{\mathrm{I}} + e^- \qquad \text{Eq. 16}$$

$$Fe^{I}_{ads} \xrightarrow{k_2} Fe^{II} + e^{-} \qquad \text{Eq. 17}$$

where k_1 and k_2 (expressed in mol cm^{-2} s^{-1}) are the rate constants of the two successive reactions. Under the assumption that the kinetic constants of the electrochemical reactions follow Tafel's law, they may be expressed as

$$k_i = k_i^0 \exp(b_i E) \qquad \text{Eq. 18}$$

where $b_i = \alpha_i(F/RT)$, α_i is the charge transfer coefficient, and E the applied potential.

Under the assumption that the adsorbate Fe^{I}_{ads} obeys a Langmuir's isotherm with Γ, the maximum number of sites per surface unit, and θ the fraction of surface coverage, the charge balance may be expressed as

$$i_F = FA[k_1(1-\theta) + k_2\theta] \qquad \text{Eq. 19}$$

where F is the Faraday constant and A is the electrode surface area. The mass balance is given as

$$\Gamma \frac{d\theta}{dt} = k_1(1-\theta) - k_2\theta \qquad \text{Eq. 20}$$

The linearization of the governing equations allows calculation of the faradaic impedance, which can be expressed as

$$\frac{1}{Z_F(\omega)} = FA\left[k_2(b_1+b_2)\theta_{stat} - (k_1-k_2)\frac{k_2(b_1-b_2)\theta_{stat}}{j\omega\Gamma+(k_1+k_2)}\right] \qquad \text{Eq. 21}$$

where θ_{stat} is the steady-state value of the fraction of surface coverage given by

$$\theta_{stat} = \frac{k_1}{k_1+k_2} \qquad \text{Eq. 22}$$

The overall impedance is then obtained by taking into account the contribution of the interfacial capacitance as a CPE contribution, and the ohmic impedance

$$Z(\omega) = R_{HF} + \frac{R_{LF}-R_{HF}}{(1+(j\omega\tau)^{\alpha})^{\beta}} + \frac{Z_F(\omega)}{1+Q(j\omega)^{\alpha}Z_F(\omega)} \qquad \text{Eq. 23}$$

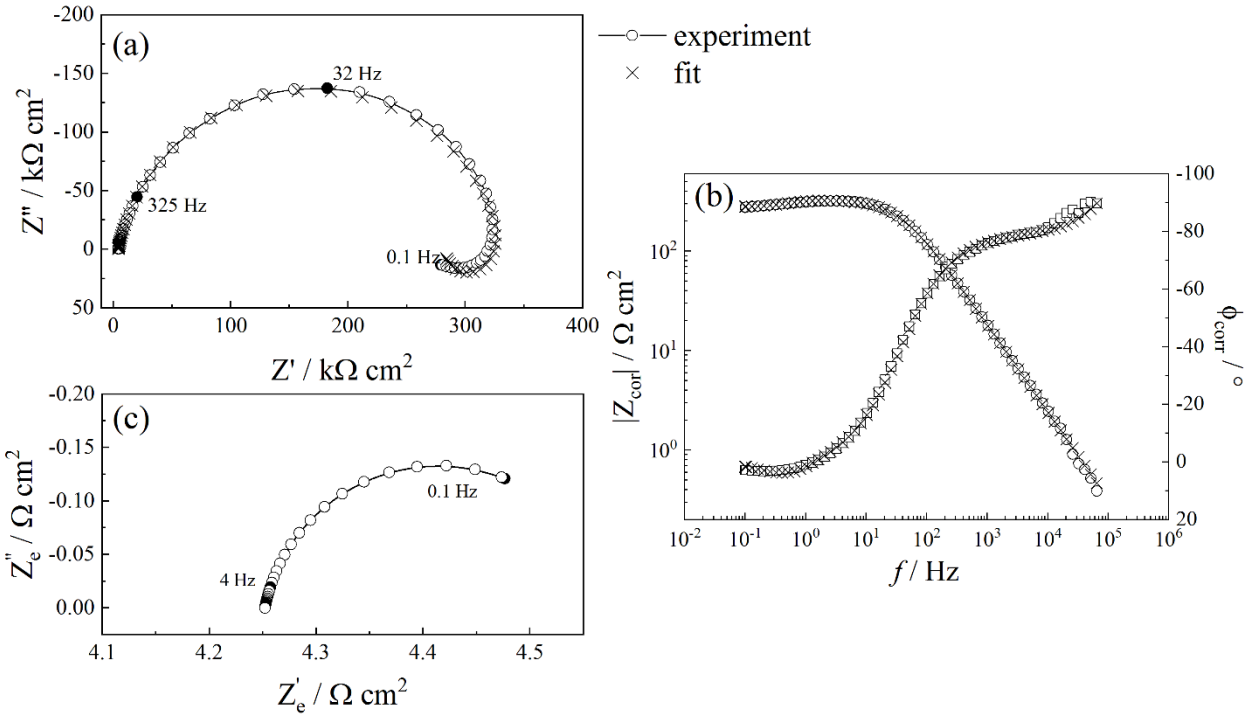

Figure 7: Electrochemical impedance response of a Fe disk-electrode of 5 mm in diameter in a 0.5 M sulfuric acid solution biased at E = -0.924 V/MSE. Nyquist representation of the impedance; (b) Bode representation of the impedance corrected by the ohmic impedance; (c) Nyquist representation of the ohmic impedance. The red symbols correspond to the experimental data and the crosses correspond to the fitting of the EIS response with the model proposed in this work (equation (23)).

Independent of the values of the different parameters obtained from the fitting procedure (which is not the aim of this analysis but are in good agreement with those reported in the literature), it is interesting to note that the high-frequency behavior of the impedance can be described by equation (23). The interfacial capacitance is in this case a CPE corresponding to the double layer in series with a partial covering thin film and is perfectly highlighted when the corrected phase is traced as a function of the frequency (Figure 7b). It is thus concluded that the high-frequency dispersion that is usually disregarded can be better interpreted by introducing the ohmic impedance that results from geometrical properties of the electrochemical system. In this case, the ohmic impedance (Figure 7c) is described by the Havriliak-Negami equation with the term $\beta = 0.77$ as parameter value.

From these results, it is thus concluded that the ohmic impedance for a disk electrode geometry can always be simulated using the Havriliak-Negami equation accounting for the high frequency dispersion. For a blocking electrode, that is for a primary steady-state current distribution, the term β of this relationship had a value between 0.65 and 0.7. When a secondary current distribution is

involved, as in the case of the active or passive dissolution, the current and potential distributions are different thus leading to β values larger than 0.68. Such a difference for the value of β between blocking and non-blocking behavior should be attributed to the fact that β corresponds to a frequency dispersion induced by the electrode geometry. For a primary current distribution, the current variation between the electrode center and the electrode edge are larger than for a secondary current distribution, thus resulting in a smaller value β for the former case.

It should be mentioned that the use of the ohmic impedance for describing the high-frequency dispersion increases the number of parameters used for the fitting procedure. However, in many cases, these parameters can be readily obtained from an appropriate graphical representation of the results, as exemplified with the different examples presented in this article.

6. Conclusions

The notion of ohmic impedance, previously developed through the development of local impedance measurements and their analysis, has been extended using both numerical and experimental results. The error made in assuming that the ohmic contribution of the impedance is only a real number depends on the system and does not necessarily interfere with the analysis of the reaction mechanisms involved at the electrode. However, as soon as the capacitive component dominates in high frequencies, the frequency dispersion distorts the electrochemical response of the interface. Thus, a suitable correction in this frequency domain is required to better highlight the CPE behavior of the interface, as shown in the examples presented, including blocking electrodes and electrochemical systems with complex kinetics involving faradaic reactions. As demonstrated in the present work, the Havriliak-Negami equation provides a universal way for describing the ohmic impedance for disk electrode geometries, independent of the system under investigation. It is also shown that if the ohmic contribution is not accurately corrected, the error on the determination of the high-frequency capacitance can be of a factor of 2.

Acknowledgement

Mark Orazem acknowledges financial support from the University of Florida Foundation Preeminence and the Dr. and Mrs. Frederick C. Edie term professorships.

References

1. Newman, J., Frequency dispersion in capacity measurements at a disk electrode. *J. Electrochem. Soc.* **1970,** *117* (2), 198-203.
2. Newman, J.; Thomas-Alyea, K. E., *Electrochemical System*. third ed.; Wiley Interscience: Hoboken, NJ, 2004.
3. Huang, V. M.-W.; Vivier, V.; Orazem, M. E.; Pebere, N.; Tribollet, B., The apparent constant-phase-element behavior of an ideally polarized blocking electrode a global and local impedance analysis. *J. Electrochem. Soc.* **2007,** *154* (2), C81-C88.
4. Huang, V. M.-W.; Vivier, V.; Frateur, I.; Orazem, M. E.; Tribollet, B., The global and local impedance response of a blocking disk electrode with local constant-phase-element behavior. *J. Electrochem. Soc.* **2007,** *154* (2), C89-C98.
5. Huang, V. M.-W.; Vivier, V.; Orazem, M. E.; Pebere, N.; Tribollet, B., The apparent constant-phase-element behavior of a disk electrode with Faradaic reactions. A global and local impedance analysis. *J. Electrochem. Soc.* **2007,** *154* (2), C99-C107.
6. Orazem, M. E.; Tribollet, B., *Electrochemical Impedance Spectroscopy*. 2 ed.; Wiley: Hoboken, New Jersey, 2017; p 768.
7. Frateur, I.; Huang, V. M.; Orazem, M. E.; Tribollet, B.; Vivier, V., Experimental Issues Associated with Measurement of Local Electrochemical Impedance. *J. Electrochem. Soc.* **2007,** *154* (12), C719-C727.
8. Bayet, E.; Huet, F.; Keddam, M.; Ogle, K.; Takenouti, H., A novel way of measuring local electrochemical impedance using a single vibrating probe. *J. Electrochem. Soc.* **1997,** *144* (4), L87-L90.
9. Bayet, E.; Huet, F.; Keddam, M.; Ogle, K.; Takenouti, H., Local electrochemical impedance measurement: scanning vibrating electrode technique in ac mode. *Electrochim. Acta* **1999,** *44* (24), 4117-4127.
10. Huang, V. M.-W.; Wu, S.-L.; Orazem, M. E.; Pebere, N.; Tribollet, B.; Vivier, V., Local electrochemical impedance spectroscopy: A review and some recent developments. *Electrochim. Acta* **2011,** *56*, 8048-8057.
11. Zou, F.; Thierry, D.; Isaacs, H. S., A high-resolution probe for localized electrochemical impedance spectroscopy measurements. *J. Electrochem. Soc.* **1997,** *144* (6), 1957-1965.
12. Blanc, C.; Orazem, M. E.; Pebere, N.; Tribollet, B.; Vivier, V.; Wu, S., The origin of the complex character of the Ohmic impedance. *Electrochim. Acta* **2010,** *55* (21), 6313-6321.
13. Frateur, I.; Huang, V. M.-W.; Orazem, M. E.; Pebere, N.; Tribollet, B.; Vivier, V., Local electrochemical impedance spectroscopy: Considerations about the cell geometry. *Electrochim. Acta* **2008,** *53* (25), 7386-7395.
14. Lopez-Quiroga, E.; Novoa, X. R.; Perez, C.; Vivier, V., Current distribution in double-cylinder electrolyte cells: Application to the study of corrosion properties of organic coatings. *Prog. Org. Coat.* **2012,** *74*, 400-404.
15. Conway, B. E., *Electrochemical Supercapacitors - Scientific Fundamentals and Technological Applications*. Kluwer Academic/Plenum Publishers: New York, 1999.
16. Harrington, S. P.; Devine, T. M., Analysis of Electrodes Displaying Frequency Dispersion in Mott-Schottky Tests. *J. Electrochem. Soc.* **2008,** *155* (8), C381.

17. Benoit, M.; Bataillon, C.; Gwinner, B.; Miserque, F.; Orazem, M. E.; Sánchez-Sánchez, C. M.; Tribollet, B.; Vivier, V., Comparison of different methods for measuring the passive film thickness on metals. *Electrochim. Acta* **2016,** *201*, 340-347.
18. Tran, T. T. M.; Tribollet, B.; Sutter, E. M. M., New insights into the cathodic dissolution of aluminium using electrochemical methods. *Electrochim. Acta* **2016,** *216*, 58-67.
19. Nguyen, A. S.; Musiani, M.; Orazem, M. E.; Pébère, N.; Tribollet, B.; Vivier, V., Impedance analysis of the distributed resistivity of coatings in dry and wet conditions. *Electrochim. Acta* **2015,** *179*, 452-459.
20. Nguyen, A. S.; Musiani, M.; Orazem, M. E.; Pébère, N.; Tribollet, B.; Vivier, V., Impedance study of the influence of chromates on the properties of waterborne coatings deposited on 2024 aluminium alloy. *Corros. Sci.* **2016,** *109*, 174-181.
21. Wu, S.-L.; Orazem, M. E.; Tribollet, B.; Vivier, V., The Influence of Coupled Faradaic and Charging Currents on Impedance Spectroscopy. *Electrochim. Acta* **2014,** *131*, 3-12.
22. Newman, J., Resistance for flow of current to a disk. *J. Electrochem. Soc.* **1966,** *113* 501-502.
23. Ngai, K. L.; Jonscher, A. K.; White, C. T., Origin of the Universal Dielectric Response in Condensed Matter. *Nature* **1979,** *277* (5693), 185-189.
24. Petrowsky, M.; Frech, R., Application of the Compensated Arrhenius Formalism to Dielectric Relaxation. *J. Phys. Chem. B* **2009,** *113* (50), 16118-16123.
25. Barsoukov, E.; Macdonald, J. R., *Impedance Spectroscopy: Theory, Experiment, and Applications*. Second ed.; John Wiley & Sons: Hoboken, NJ., 2005; p xvii + 596 pp.
26. Havriliak, S.; Negami, S., A complex plane representation of dielectric and mechanical relaxation processes in some polymers. *Polymer* **1967,** *8*, 161-210.
27. Orazem, M. E.; Pebere, N.; Tribollet, B., Enhanced Graphical Representation of Electrochemical Impedance Data. *J. Electrochem. Soc.* **2006,** *153* (4), B129-B136.
28. Jurczakowski, R.; Hitz, C.; Lasia, A., Impedance of porous Au based electrodes. *J. Electroanal. Chem.* **2004,** *572* (2), 355-366.
29. Brug, G. J.; van den Eeden, A. L. G.; Sluyters-Rehbach, M.; Sluyters, J. H., The analysis of electrode impedances complicated by the presence of a constant phase element. *J. Electroanal. Chem.* **1984,** *176* (1-2), 275-295.
30. Hirschorn, B.; Orazem, M. E.; Tribollet, B.; Vivier, V.; Frateur, I.; Musiani, M., Determination of effective capacitance and film thickness from constant-phase-element parameters. *Electrochim. Acta* **2010,** *55* (21), 6218-6227.
31. Hirschorn, B.; Orazem, M. E.; Tribollet, B.; Vivier, V.; Frateur, I.; Musiani, M., Constant-Phase-Element Behavior Caused by Resistivity Distributions in Films: II. Applications. *J. Electrochem. Soc.* **2010,** *157* (12), C458-C463.
32. Hirschorn, B.; Orazem, M. E.; Tribollet, B.; Vivier, V.; Frateur, I.; Musiani, M., Constant-Phase-Element Behavior Caused by Resistivity Distributions in Films: I. Theory. *J. Electrochem. Soc.* **2010,** *157* (12), C452-C457.
33. Gomes, M. P.; Costa, I.; Pébère, N.; Rossi, J. L.; Tribollet, B.; Vivier, V., On the corrosion mechanism of Mg investigated by electrochemical impedance spectroscopy. *Electrochim. Acta* **2019,** *306*, 61-70.
34. Bockris, J. O. M.; Drazic, D.; Despic, A. R., The electrode kinetics of the deposition and dissolution of iron. *Electrochim. Acta* **1961,** *4*, 325-361.

35. Epelboin, I.; Keddam, M.; Lestrade, J. C., Faradaic impedances and intermediates in electrochemical reactions. *Faraday Discuss. Chem. Soc.* **1973,** *56*, 264-75.